
ARTIFICIAL INTELLIGENCE-DERIVED VASCULAR AGE FROM PHOTOPLETHYSMOGRAPHY: A NOVEL DIGITAL BIOMARKER FOR CARDIOVASCULAR HEALTH

A PREPRINT

Guangkun Nie^{1,2}, Qinghao Zhao³, Gongzheng Tang^{1,2}, Yaxin Li¹, Shenda Hong^{1,2,4,5,6,*}

¹Institute of Medical Technology, Health Science Center of Peking University, Beijing, China

²National Institute of Health Data Science, Peking University, Beijing, China

³Department of Cardiology, Peking University People's Hospital, Beijing, China

⁴Institute for Artificial Intelligence, Peking University, Beijing, China

⁵Department of Emergency Medicine, Peking University First Hospital, Beijing, China

⁶NHC Key Laboratory of Cardiovascular Molecular Biology and Regulatory Peptides, Peking University, Beijing, China

February 20, 2025

ABSTRACT

With the increasing availability of wearable devices, photoplethysmography (PPG) has emerged as a promising non-invasive tool for monitoring human hemodynamics. Leveraging this potential, we present a deep learning-based framework to directly estimate vascular age (AI-vascular age) from PPG signals, incorporating a novel distribution-aware loss function to address biases caused by imbalanced data distributions. We further explore AI-vascular age as a digital biomarker for cardiovascular health assessment. The model was developed and evaluated using data from the UK Biobank (UKB) cohort. The development cohort consisted of 98,672 data pairs from 98,672 participants without a history of circulatory disorders, diabetes, or dyslipidemia, while 144,683 data pairs from 113,559 participants were reserved for clinical evaluation. After adjusting for key confounding factors, including age, sex, ethnicity, and body mass index, results showed that participants with a vascular age gap (AI-vascular age minus calendar age) exceeding 9 years had a significantly higher risk of the primary outcome, major adverse cardiovascular and cerebrovascular events (MACCE) (HR = 2.37, $p < 0.005$). They also exhibited an elevated risk of secondary outcomes, including diabetes (HR = 2.69, $p < 0.005$), hypertension (HR = 2.88, $p < 0.005$), coronary heart disease (HR = 2.20, $p < 0.005$), heart failure (HR = 2.15, $p < 0.005$), myocardial infarction (HR = 2.51, $p < 0.005$), stroke (HR = 2.55, $p < 0.005$), and all-cause mortality (HR = 2.51, $p < 0.005$). Conversely, participants with a vascular age gap below -9 years exhibited a significantly lower incidence of these outcomes. We further evaluated the longitudinal applicability of AI-vascular age using serial PPG data from the UKB, demonstrating its value in risk stratification by leveraging AI-vascular age at two distinct time points to predict future MACCE incidence. External validation was performed on a MIMIC-III-derived cohort ($n = 2,343$), where each one-year increase in vascular age gap was significantly associated with elevated in-hospital mortality risk (OR = 1.02, $p < 0.005$). In conclusion, our study establishes AI-vascular age as a novel, non-invasive digital biomarker for cardiovascular health assessment. By transforming PPG signals into actionable insights, this approach offers significant potential for scalable risk stratification, personalized health monitoring, and early intervention in both general and high-risk populations.

1 Introduction

Cardiovascular diseases (CVDs) are the leading cause of global mortality and a major contributor to reduced quality of life Roth et al. [2018], Cooper [2018], Mensah et al. [2019]. In 2021, an estimated 621 million individuals worldwide

were affected by CVDs, resulting in approximately 20.5 million deaths Lindstrom et al. [2022]. Early risk identification and timely intervention are crucial for improving outcomes and preventing disease progression van Daalen et al. [2024]. However, existing screening and diagnostic methods primarily depend on specialized healthcare professionals and facility-based equipment Vogel et al. [2021], Pandey et al. [2025], Addissouky et al. [2024], which limits accessibility, particularly in resource-constrained settings. Moreover, the lack of simple, user-friendly tools for cardiovascular risk assessment outside clinical environments hinders timely monitoring and proactive health management. This gap affects not only individuals already diagnosed with CVDs but also those at elevated risk who could benefit from earlier intervention. These challenges highlight the pressing need for accessible, cost-effective solutions that provide clear, actionable insights into cardiovascular health, enabling individuals to conveniently monitor their risk and promoting the broader adoption of preventive care strategies.

Recent advancements in sensor technology and data analytics have significantly broadened the potential applications of photoplethysmography (PPG) signals. PPG is a non-invasive and easily accessible optical physiological signal that can effectively monitor hemodynamic parameters, such as heart rate Pankaj et al. [2022] and blood oxygen saturation Schröder et al. [2023], and has been widely integrated into wearable devices including smartwatches Pereira et al. [2020], Williams et al. [2023], Krittanawong et al. [2021]. With the growth of artificial intelligence (AI), the application of PPG in CVDs, such as atrial fibrillation Yang et al. [2019], Pereira et al. [2020] and hypertension Elgendi et al. [2019], Mousavi et al. [2019], has gained increasing attention. Studies have shown that vascular aging, which leads to increased arterial stiffness, is closely associated with a heightened risk of CVDs Vasani et al. [2019, 2022] and induces characteristic changes in PPG waveforms Li et al. [2022], Chen et al. [2024]. Given this relationship, it is conceivable to extract quantitative biomarkers from PPG signals that can assess the extent of vascular aging and be used for cardiovascular health evaluation and management.

Building on the success of AI-driven digital biomarkers, such as AI-ECG age Lima et al. [2021], Park et al. [2024], Hempel et al. [2025], we hypothesize that deep learning methods can be applied to predict vascular age (AI-vascular age) directly from PPG signals. Vascular age, in this context, represents a biological age that more accurately reflects the degree of vascular aging compared to calendar age, providing a more reliable indicator of vascular health. In healthy individuals, vascular age typically aligns with calendar age, with their PPG signals corresponding to this expected range. Conversely, individuals with CVDs often exhibit a vascular age exceeding their calendar age due to increased arterial stiffness, resulting in PPG signals that resemble those of older individuals. Based on this concept, a deep learning model trained to predict calendar age from PPG signals in healthy individuals could be adapted to estimate vascular age, offering a novel approach for assessing vascular health.

In this study, we propose a deep learning-based approach to predict vascular age directly from PPG signals. To address the challenge of imbalanced age distribution in the training data, we introduce a novel distribution-aware loss function to mitigate this issue (Figure 1). The model was developed and evaluated using the UK Biobank (UKB) dataset. Our results demonstrate that the vascular age gap, defined as the difference between AI-vascular age and calendar age, serves as an independent risk factor for the primary outcome of major adverse cardiovascular events (MACCE) as well as for secondary outcomes, including diabetes, hypertension, coronary heart disease (CHD), heart failure (HF), myocardial infarction (MI), stroke, and all-cause mortality. Additionally, we assessed the longitudinal utility of AI-vascular age by analyzing serial PPG data from the same individuals over time. External validation on a MIMIC-III-derived dataset further confirmed a significant positive correlation between the vascular age gap and in-hospital mortality. These findings highlight the potential of AI-vascular age as a valuable tool for cardiovascular health monitoring and risk management.

2 Results

2.1 Deep learning model for vascular age prediction

In this study, we developed and evaluated our model using the UKB dataset, PulseDB, and the MIMIC-III Clinical Database (Table 1). The data flow across these datasets is depicted in Figure 2. The UKB dataset contains 243,355 PPG recordings from 212,231 participants and is divided into a development cohort (98,672 PPGs from 98,672 participants) and a clinical evaluation cohort (144,683 PPGs from 113,559 participants). Exclusion criteria for the development cohort were applied at the participant level to prevent data leakage: 1) participants with multiple assessment visits resulting in multiple PPG recordings, and 2) participants with a history of circulatory system disorders, diabetes, or dyslipidemia at the time of assessment. Circulatory disorders were identified according to UKB category 2409. The first criterion preserved serial PPG data for longitudinal analysis of AI-vascular age, while the second ensured that vascular age in the training data aligned with calendar age for label integrity. The development cohort was then partitioned into training, selection, and hold-out sets in an 8:1:1 ratio. The selection set was used for model selection, and the hold-out set evaluated the model’s ability to predict vascular age. The clinical evaluation cohort was used to assess the

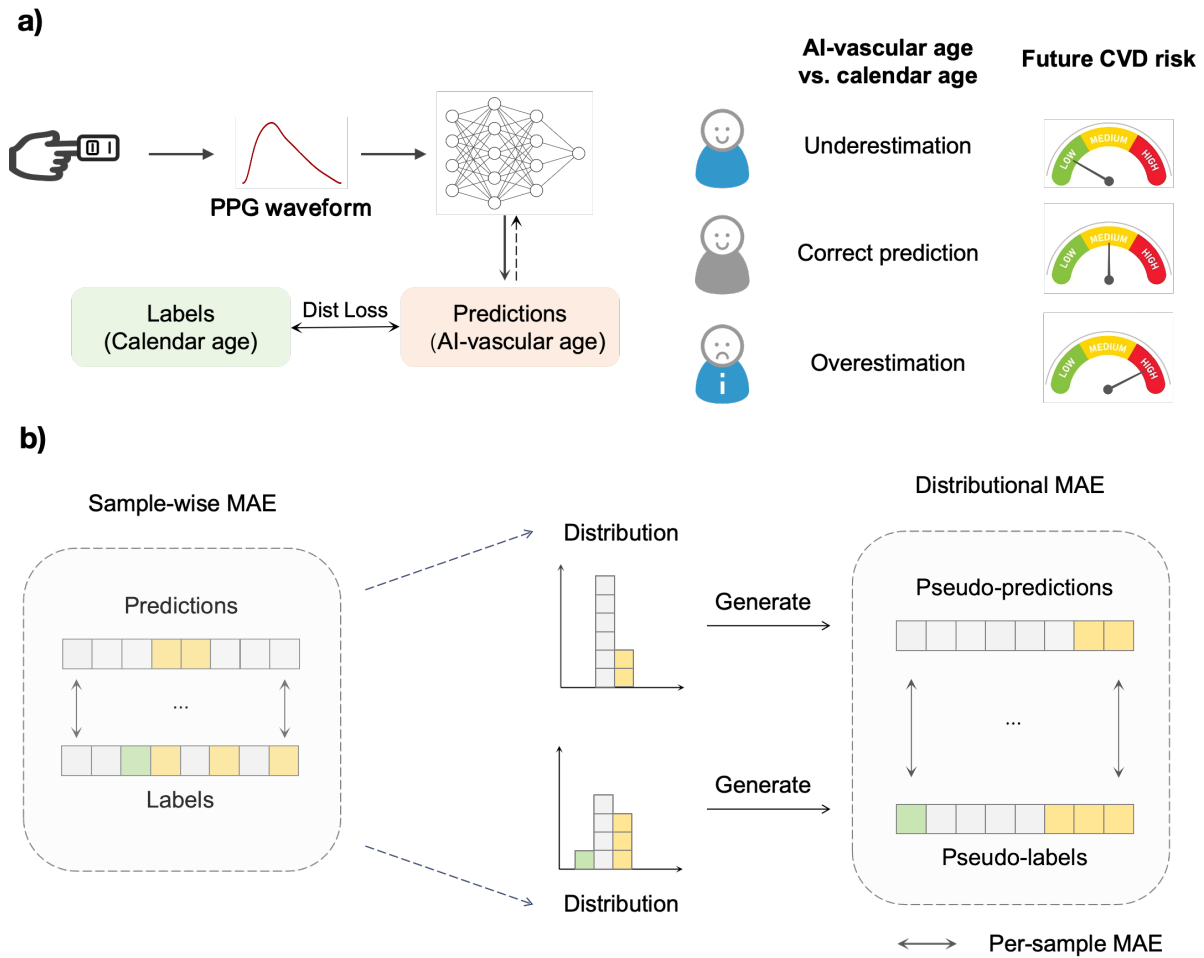


Figure 1: Development and application of the vascular age prediction model. a) We employ a deep learning model to predict vascular age directly from PPG waveforms. A higher vascular age gap, defined as the difference between AI-vascular age and calendar age, is associated with an increased risk of future CVDs. b) In the training phase, we introduce Dist Loss to address the imbalanced regression problem. Dist Loss comprises two components: sample-wise MAE and distributional MAE. The sample-wise MAE quantifies the discrepancy between predictions and ground truth labels, while the distributional MAE captures the divergence between their respective distributions. To illustrate the core concept behind distributional MAE, the figure simplifies its computation by assuming that the batch size equals the total number of training samples. CVDs, cardiovascular diseases; MAE, mean absolute error.

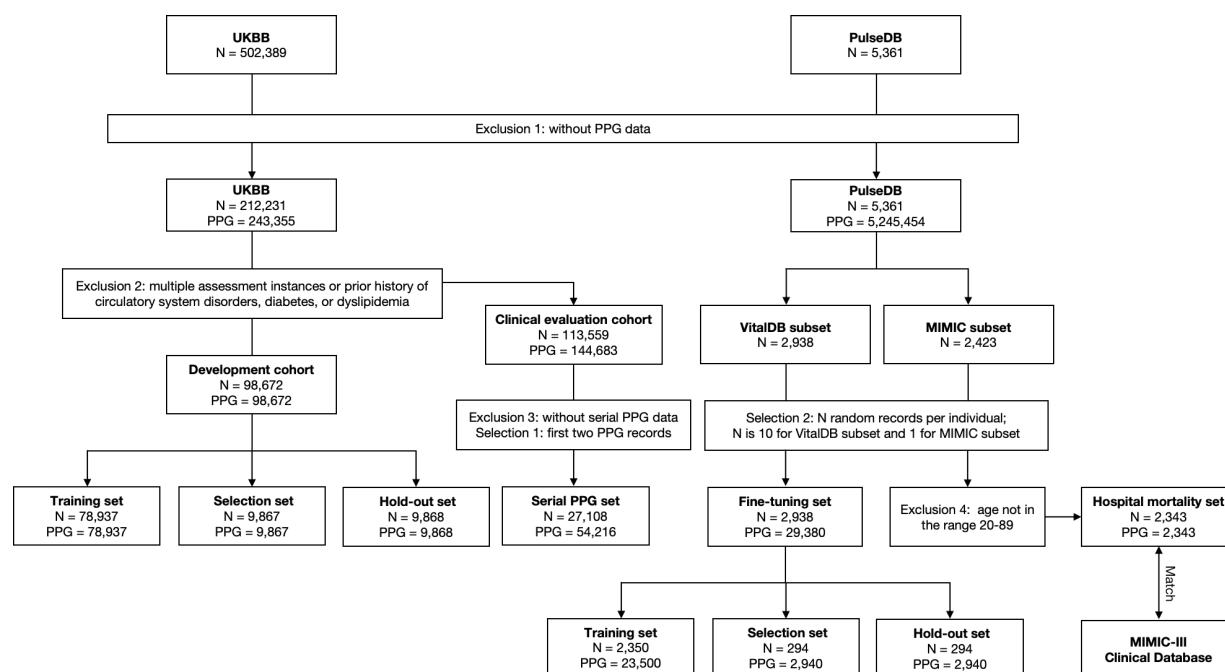


Figure 2: Data flow chart. The vascular age prediction model was developed and evaluated using the UKB dataset. The VitalDB subset of the PulseDB dataset was used to fine-tune the UKB-trained model, while the MIMIC subset of the PulseDB dataset was linked to the MIMIC-III Clinical Database for external evaluation. UKB: UK Biobank.

predictive capability of AI-vascular age for future clinical events. A subset with serial PPG recordings ($N = 27,108$, $PPG = 54,216$) was extracted to form the serial PPG set for longitudinal analysis.

The PulseDB dataset ($N = 5,361$, $PPG = 5,245,454$) comprises the VitalDB and MIMIC subsets. For the VitalDB subset, up to ten PPG recordings were randomly selected for each patient to construct a fine-tuning set ($N = 2,938$, $PPG = 29,380$). If a patient had fewer than ten recordings, random duplication was applied to reach ten recordings. This fine-tuning set was split into training, selection, and hold-out sets in an 8:1:1 ratio to adapt the UKB-trained model for temporal variations across datasets. In the MIMIC subset, one PPG recording per patient was selected for vascular age prediction and linked to the MIMIC-III Clinical Database to create the MIMIC hospital mortality set ($N = 2,343$, $PPG = 2,343$). Given the distinct data sources of the MIMIC and VitalDB subsets, the entire MIMIC hospital mortality set was reserved for external evaluation of the fine-tuned model.

The performance of the vascular age prediction model was evaluated on the UKB hold-out set, UKB clinical evaluation set, VitalDB hold-out set, and MIMIC hospital mortality set, with detailed results shown in Table 2. In the UKB hold-out set, the Pearson correlation coefficient between AI-vascular age and calendar age was 0.49, with a mean absolute error (MAE) of 7.57 years. In the clinical evaluation set, the correlation was 0.38, with an MAE of 8.18 years, likely due to the inclusion of individuals with existing CVDs, resulting in greater inconsistency between vascular age and calendar age. For the VitalDB hold-out set, the correlation was 0.54 with an MAE of 9.69 years. In the MIMIC hospital mortality set, the correlation dropped to 0.41, with an MAE of 11.81 years, reflecting the greater heterogeneity and hemodynamic instability in ICU patients, which may have contributed to the reduced performance.

2.2 Vascular age gap as a predictor of major adverse cardiovascular and cerebrovascular events and cardiometabolic diseases

We utilized the Cox proportional hazards model to assess whether the vascular age gap serves as an independent risk factor for future MACCE, which was designated as the primary outcome in this study. In addition, we explored its association with several secondary outcomes, including diabetes, hypertension, CHD, HF, MI, stroke, and all-cause mortality. To provide a comprehensive evaluation of the predictive value of the vascular age gap, we analyzed it both as a continuous and categorical variable. Two levels of covariate adjustment were applied: Model 1 adjusted for age, sex, ethnicity, and body mass index (BMI), while Model 2 incorporated further adjustments for smoking status, hypertension, diabetes, dyslipidemia, and chronic kidney disease (CKD).

Table 1: Clinical characteristics. UKB, UK Biobank; MACCE: major cardiovascular and cerebrovascular events; NA, not available.

Characteristics	UKB		MIMIC subset
	Development cohort (N=98,672)	Clinical evaluation cohort (N=144,683)	Hospital mortality set (N=2,343)
Age (years)	55.81±8.63	60.87±8.03	61.51±15.25
Sex	N=98,672	N=144,683	N=2,343
Male	40,797 (41.35%)	73,203 (50.60%)	1,376 (58.73%)
Female	57,875 (58.65%)	71,480 (49.40%)	967 (41.27%)
Race	N=98,065	N=143,959	N=2,005
White	90,398 (92.18%)	134,717 (93.58%)	1,668 (83.19%)
Asian	3,329 (3.39%)	4,344 (3.02%)	47 (2.34%)
Black	2,287 (2.33%)	2,750 (1.91%)	191 (9.53%)
Mixed	829 (0.85%)	792 (0.55%)	6 (0.30%)
Others	1,222 (1.25%)	1,356 (0.94%)	93 (4.64%)
BMI (kg/m ²)	26.46±4.36	27.79±4.92	29.41±9.91
Hypertension	0 (0%)	69,682 (48.16%)	1,383 (59.03%)
Diabetes	0 (0%)	14,099 (9.74%)	673 (28.72%)
Dyslipidemia	0 (0%)	45,535 (31.47%)	805 (34.36%)
Chronic kidney disease	454 (0.46%)	3639 (2.52%)	362 (15.45%)
Smoking status	N=98,083	N=143,648	
None-smoker	88,238 (89.96%)	133608 (93.01%)	2,073 (88.48%)
Current smoking	9,845 (10.04%)	10,040 (6.99%)	270 (11.52%)
Heart Failure	0 (0%)	1,517 (1.05%)	559 (23.86%)
Myocardial infarction	8 (0.01%)	5,745 (3.97%)	383 (16.35%)
Stroke	11 (0.01%)	3,440 (2.38%)	323 (13.79%)
Coronary heart disease	0 (0%)	14,038 (9.70%)	662 (28.25%)
MACCE	19 (0.02%)	17,278 (11.94%)	1,132 (48.31%)
Follow-up time (years)	11.66 (3.10)	9.87 (3.23)	NA

Table 2: Performance of the vascular age prediction model. UKB, UK Biobank; MAE, mean absolute error.

Datasets	Pearson correlation coefficient	MAE (years)
UKB hold-out set	0.49	7.57
UKB clinical evaluation set	0.38	8.18
VitalDB hold-out set	0.54	9.60
MIMIC hospital mortality set	0.41	11.81

Table 3: Adjusted HRs for future MACCE and cardiometabolic diseases. The vascular age gap is evaluated both as a continuous variable and as a categorical variable. For the categorical analysis, participants are classified into three groups: underestimation, correct prediction, and overestimation, with the correct prediction group serving as the reference. HR, hazard ratio; MACCE, major adverse cardiovascular and cerebrovascular events; BMI, body mass index.

Cardiovascular event	Vascular age gap		Underestimation		Overestimation	
	HR (95% CI)	p-value	HR (95% CI)	p-value	HR (95% CI)	p-value
Model 1, adjusted by age, sex, ethnicity and BMI						
MACCE	1.02 (1.02-1.03)	<0.005	0.79 (0.77-0.82)	<0.005	2.37 (2.17-2.59)	<0.005
Diabetes	1.04 (1.04-1.05)	<0.005	0.68 (0.64-0.72)	<0.005	2.69 (2.42-2.99)	<0.005
Hypertension	1.05 (1.05-1.05)	<0.005	0.62 (0.59-0.64)	<0.005	2.88 (2.66-3.11)	<0.005
Coronary heart disease	1.03 (1.03-1.04)	<0.005	0.71 (0.68-0.74)	<0.005	2.20 (2.00-2.42)	<0.005
Heart failure	1.02 (1.02-1.02)	<0.005	0.82 (0.77-0.87)	<0.005	2.15 (1.82-2.54)	<0.005
Myocardial infraction	1.04 (1.03-1.04)	<0.005	0.69 (0.64-0.73)	<0.005	2.51 (2.17-2.91)	<0.005
Stroke	1.03 (1.02-1.03)	<0.005	0.78 (0.72-0.85)	<0.005	2.55 (2.11-3.08)	<0.005
All-cause mortality	1.02 (1.02-1.02)	<0.005	0.86 (0.82-0.90)	<0.005	2.51 (2.22-2.84)	<0.005
Model 2, adjusted by age, sex, ethnicity, BMI, smoking status, hypertension, diabetes, dyslipidemia, and CKD						
MACCE	1.02 (1.02-1.02)	<0.005	0.82 (0.79-0.85)	<0.005	2.24 (2.05-2.45)	<0.005
Coronary heart disease	1.03 (1.03-1.03)	<0.005	0.72 (0.69-0.76)	<0.005	2.13 (1.94-2.35)	<0.005
Heart failure	1.02 (1.01-1.02)	<0.005	0.84 (0.79-0.89)	<0.005	2.08 (1.76-2.46)	<0.005
Myocardial infraction	1.03 (1.03-1.04)	<0.005	0.70 (0.66-0.75)	<0.005	2.41 (2.08-2.79)	<0.005
Stroke	1.02 (1.02-1.03)	<0.005	0.80 (0.74-0.87)	<0.005	2.41 (2.00-2.91)	<0.005
All-cause mortality	1.02 (1.01-1.02)	<0.005	0.89 (0.85-0.94)	<0.005	2.35 (2.07-2.66)	<0.005

In Model 1, restricted cubic spline curves (Figure 3) were used to illustrate the relationship between the vascular age gap (as a continuous variable) and the risk of MACCE as well as secondary outcomes. As shown, hazard ratios (HRs) progressively increased with the vascular age gap. Table 3 presents the HRs for each one-year increase in the vascular age gap. Notably, significant associations were observed not only for the primary outcome, MACCE (HR = 1.02, $p < 0.005$), but also for all secondary outcomes: diabetes (HR = 1.04, $p < 0.005$), hypertension (HR = 1.05, $p < 0.005$), CHD (HR = 1.03, $p < 0.005$), HF (HR = 1.02, $p < 0.005$), MI (HR = 1.04, $p < 0.005$), stroke (HR = 1.03, $p < 0.005$), and all-cause mortality (HR = 1.02, $p < 0.005$). The trends observed in Model 2 were consistent, with HRs remaining statistically significant for all outcomes.

To further investigate the vascular age gap, the study population was stratified into three groups based on the gap: underestimation (< -9 years), correct prediction (-9 to 9 years), and overestimation (> 9 years). The correct prediction group was used as the reference group. We then evaluated the relative risks of future MACCE and secondary outcomes in both the underestimation and overestimation groups. The results, summarized in Table 3, revealed that the underestimation group had a significantly lower risk for MACCE (HR = 0.79, $p < 0.005$) as well as all secondary outcomes, including diabetes (HR = 0.68, $p < 0.005$), hypertension (HR = 0.62, $p < 0.005$), CHD (HR = 0.71, $p < 0.005$), HF (HR = 0.82, $p < 0.005$), MI (HR = 0.69, $p < 0.005$), stroke (HR = 0.78, $p < 0.005$), and all-cause mortality (HR = 0.86, $p < 0.005$). In contrast, the overestimation group exhibited a significantly higher risk for MACCE (HR = 2.37, $p < 0.005$) and all secondary outcomes, including diabetes (HR = 2.69, $p < 0.005$), hypertension (HR = 2.88, $p < 0.005$), CHD (HR = 2.20, $p < 0.005$), HF (HR = 2.15, $p < 0.005$), MI (HR = 2.51, $p < 0.005$), stroke (HR = 2.55, $p < 0.005$), and all-cause mortality (HR = 2.51, $p < 0.005$). These results were consistent in Model 2, where statistical significance was maintained for all outcomes.

Finally, Kaplan-Meier (KM) curves (Figure 4) were employed to illustrate the cumulative incidence of MACCE and secondary outcomes across the three vascular age gap groups. The findings highlight the vascular age gap as a robust predictor of MACCE and underscore its potential utility in cardiovascular risk stratification.

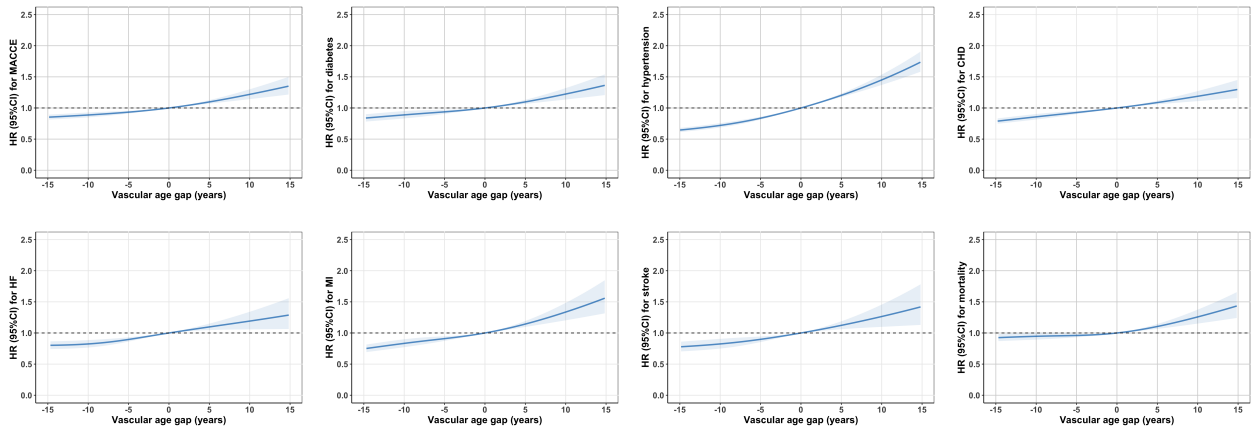


Figure 3: Spline curves illustrating the risk of MACCE and cardiometabolic diseases as the vascular age gap increases. MACCE, major adverse cardiovascular and cerebrovascular events.

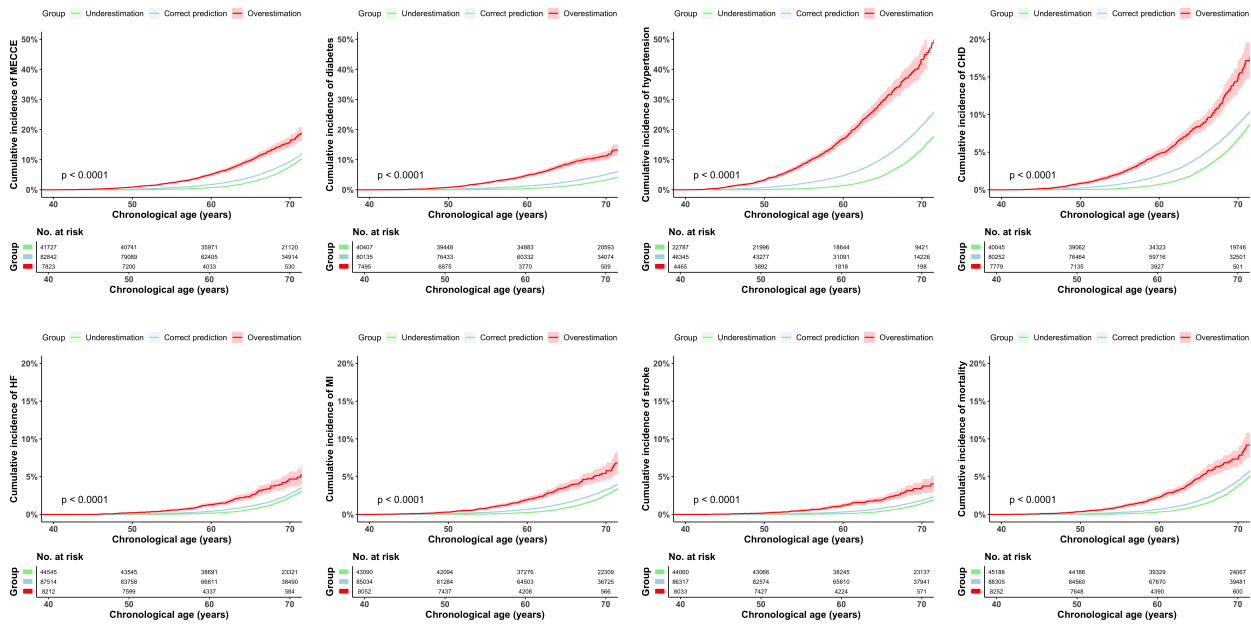


Figure 4: KM curves illustrating the cumulative incidence of MACCE and cardiometabolic diseases across three groups: overestimation, correct prediction, and underestimation. KM, Kaplan-Meier; MACCE, major adverse cardiovascular and cerebrovascular events.

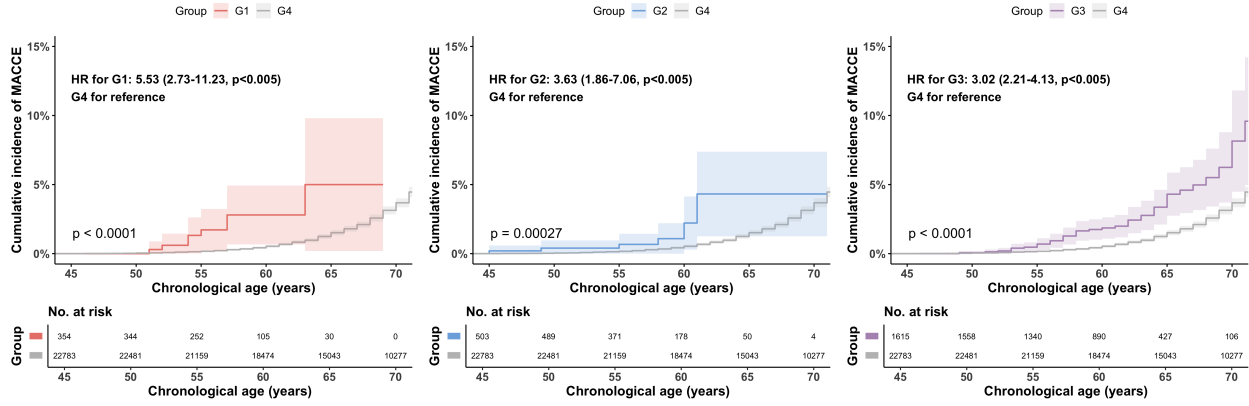


Figure 5: KM curves for future MACCE based on vascular age gap classifications from serial PPG measurements at two time points. Group G4 (reference) represents individuals with both measurements classified as correct prediction or underestimation. Group G1 includes individuals with both measurements classified as overestimation, Group G2 includes those with the first measurement classified as underestimation or correct prediction and the second as overestimation, and Group G3 includes those with the first measurement classified as overestimation and the second as underestimation or correct prediction. The KM curves compare G1, G2, and G3 to the reference group (G4), with corresponding HRs indicated on each plot. KM, Kaplan-Meier; MACCE: major adverse cardiovascular and cerebrovascular events; HR: hazard ratio.

2.3 Vascular age gap classification over time based on serial PPG data is associated with future risk of major adverse cardiovascular and cerebrovascular events

The results based on serial PPG measurements at two time points are shown in Fig. 5. Group G4 (both measurements classified as correct prediction or underestimation) served as the reference. The KM curves and corresponding HRs for future MACCE are presented for Group G1 (both measurements classified as overestimation), Group G2 (first measurement classified as underestimation or correct prediction, second as overestimation), and Group G3 (first measurement classified as overestimation, second as underestimation or correct prediction). The HRs were 5.53 (95% CI: 2.73–11.23, $p < 0.005$) for Group G1, 3.63 (95% CI: 1.86–7.06, $p < 0.005$) for Group G2, and 3.02 (95% CI: 2.21–4.13, $p < 0.005$) for Group G3. The log-rank test p -values for comparisons of G1, G2, and G3 with the reference group G4 were all < 0.001 , indicating significant differences. Notably, the HRs were consistently higher than 1 and showed an increasing trend from Group G3 to Group G1, suggesting that changes in vascular age gap classification over time may provide additional value beyond single-time-point assessments.

2.4 Higher vascular age gap correlates with increased in-hospital mortality

In the external validation using the MIMIC hospital mortality set, we evaluated the association between vascular age gap and in-hospital mortality. Vascular age gap was analyzed both as a continuous variable and a categorical variable (Table 4). For the categorical analysis, underestimation and overestimation were defined using a threshold of 15 years, based on the standard deviation of the overall prediction error.

After adjusting for age, sex, and ethnic background, vascular age gap as a continuous variable was significantly associated with in-hospital mortality, with a HR of 1.02 per one-year increase (95% CI: 1.01–1.03, $p = 0.007$). When treated as a categorical variable, underestimation showed no significant difference compared to the correct prediction group (HR: 0.97, $p = 0.85$). In contrast, overestimation was associated with a significantly higher risk of in-hospital mortality (HR: 1.82, $p < 0.005$). These findings suggest that a greater vascular age gap, particularly in cases of overestimation, is linked to an elevated risk of in-hospital mortality.

2.5 AI-vascular age model demonstrates consistent focus on key PPG features across age groups

Figure 6 presents the average PPG waveforms and corresponding saliency maps for three distinct age groups (40, 55, and 70 years old). In the saliency maps, regions with higher brightness indicate areas that attract more attention from the model and are therefore more influential in the prediction process. The saliency maps show that, across all age groups, the model consistently focuses on the region surrounding the diastolic peak, with secondary attention directed towards the systolic peak. This suggests that the model relies on these two key features in the PPG waveform for

Table 4: Association between vascular age gap and in-hospital mortality in the MIMIC hospital mortality set. Vascular age gap is analyzed as a continuous variable, while underestimation and overestimation are categorized relative to the correct prediction group, adjusted for age, sex, and ethnicity. HR, hazard ratio.

	Vascular age gap		Underestimation		Overestimation	
	HR (95% CI)	p-value	HR (95% CI)	p-value	HR (95% CI)	p-value
In-hospital mortality	1.02 (1.01–1.03)	0.007	0.97 (0.73–1.29)	0.85	1.82 (1.20–2.74)	<0.005

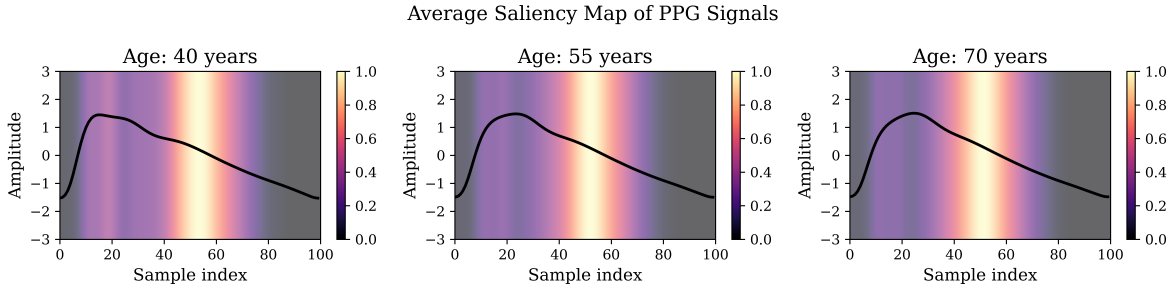


Figure 6: Averaged PPG signals and corresponding saliency maps across three age groups (40, 55, and 70 years old). Each column represents the averaged PPG signal and its associated saliency map for the respective age group.

vascular age prediction. Correspondingly, the average PPG waveforms exhibit age-related changes, particularly in the diastolic and systolic peaks. As age increases, the distance between the two peaks narrows, and the prominence of the diastolic peak gradually diminishes. These observed trends in the PPG waveforms closely match the areas of attention highlighted in the saliency maps, which is consistent with findings in existing literature Yousef et al. [2012], Lin et al. [2023]. This alignment further supports the model’s ability to identify features related to vascular aging in the PPG signals, contributing to accurate vascular age estimation.

3 Methods

3.1 Datasets

UK Biobank cohort The UKB is a large-scale biomedical resource comprising de-identified genetic, lifestyle, and health data, along with biological samples, from over 500,000 participants across the United Kingdom Sudlow et al. [2015]. The cohort includes four assessment instances: the initial assessment visit (2006–2010) with 502,150 participants, the first repeat assessment visit (2012–2013) with 20,337 participants, the imaging visit (2014–present) with 90,683 participants, and the first repeat imaging visit (2019–present) with 12,734 participants. Longitudinal follow-up data are also available, enabling comprehensive tracking of participants’ health over time. In this study, PPG signals were extracted from UKB field 4205, and corresponding age information was obtained from UKB field 21003. The PPG signals were recorded using the PulseTrace PCA2 device, with each signal preprocessed and provided by UKB in a standardized format containing 100 sample points per waveform.

PulseDB Dataset PulseDB is a curated dataset designed specifically for benchmarking cuff-less blood pressure estimation methods Wang et al. [2023]. It contains high-quality 10-second PPG segments sampled at 125 Hz from 5,361 subjects, accompanied by demographic information such as age. The dataset consists of two primary subsets: the MIMIC-III subset ($n=2,423$) and the VitalDB subset ($n=2,938$). The MIMIC-III subset includes PPG data from patients admitted to the critical care units at Beth Israel Deaconess Medical Center between 2001 and 2012 Johnson et al. [2016a], while the VitalDB subset comprises PPG recordings from surgical patients undergoing routine or emergency procedures at Seoul National University Hospital, Republic of Korea Lee et al. [2022]. In this study, the VitalDB subset was used to fine-tune the vascular age prediction model initially developed on the UKB dataset. This fine-tuning step was necessary to account for potential temporal and population-level differences between the UKB and PulseDB datasets, ensuring better generalization and adaptability of the model to new data sources., while the MIMIC-III subset was employed for external validation. Furthermore, the MIMIC-III subset within PulseDB was linked to the MIMIC-III Clinical Database Johnson et al. [2016b] to obtain corresponding in-hospital mortality data for additional analysis.

Given the high quality of the PPG data in both the UKB and PulseDB datasets, minimal preprocessing was required. Z-score normalization was applied to standardize the signals and ensure consistency across subjects, aligning input data distributions for robust model training.

3.2 Model development

3.2.1 Model architecture

The vascular age prediction model is based on Net1D Hong et al. [2020], a one-dimensional convolutional neural network (CNN) built on a ResNet He et al. [2016] variant. It is selected for its ability to capture subtle and discriminative patterns in PPG signals related to vascular aging. Net1D employs sequential convolutional blocks with residual connections He et al. [2016] and squeeze-and-excitation (SE) modules Hu et al. [2018] to enhance feature extraction. The residual connections mitigate model degradation and stabilize training, while the SE modules adaptively recalibrate channel-wise feature responses to emphasize relevant vascular aging features. This architecture ensures robust and efficient processing of PPG signals for vascular age prediction.

3.2.2 Imbalanced regression in vascular age prediction

In vascular age prediction using the UKB dataset, a significant challenge arises from the highly imbalanced age distribution. Most samples are concentrated within the age range of 50 (second decile) to 69 (ninth decile) years, while the tail regions (37–49 and 70–87 years) contain relatively few samples. Conventional loss functions, such as the MAE, treat all samples equally. Consequently, models trained with these loss functions tend to focus excessively on the majority age group. This causes samples in sparsely populated regions to be biased toward the dense central region, resulting in a pronounced deviation between the distribution of model predictions and the true label distribution. To address this issue, we propose Dist Loss, a distribution-aware loss function that enhances performance in underrepresented regions without sacrificing overall accuracy. The central idea of Dist Loss is to align the distribution of model predictions with the true label distribution, thereby ensuring accurate predictions across all age groups (Figure 1).

The technical details of Dist Loss are described below. Dist Loss comprises two main components: the sample-wise MAE and the distributional MAE. The sample-wise MAE is equivalent to the conventional MAE loss and computes the absolute error between each prediction and its corresponding ground truth, ensuring individual sample accuracy. The distributional MAE, on the other hand, quantifies the discrepancy between the distribution of model predictions and the true label distribution. It is optimized by minimizing the MAE between a pseudo-label sequence (constructed based on the label distribution) and a pseudo-prediction sequence (obtained by sorting the model predictions).

Specifically, we first employ kernel density estimation (KDE) Parzen [1962] to obtain a smooth approximation of the label distribution across the dataset. For each label y_i , a probability p_i is estimated to reflect its overall frequency. For a batch of size B , the expected frequency of y_i is given by $n_i = B \cdot p_i$. Since n_i is generally non-integer, we take its floor value $\lfloor n_i \rfloor$. To ensure that the total frequency matches the batch size B , we compute the residual $r = B - \sum_{i=1}^L \lfloor n_i \rfloor$, where L denotes the number of unique labels. An auxiliary sequence $\mathcal{R} = (r_1, r_2, \dots, r_L)$ is then defined as

$$r_i = \begin{cases} 1, & \text{if } i \leq \lfloor \frac{r+1}{2} \rfloor \text{ or } i > B - \lfloor \frac{r}{2} \rfloor, \\ 0, & \text{otherwise,} \end{cases}$$

which distributes the residual across the labels. The adjusted frequency for each label is given by $n'_i = \lfloor n_i \rfloor + r_i$, ensuring that $\sum_{i=1}^L n'_i = B$. Using these adjusted frequencies, we construct the pseudo-label sequence $\mathcal{S}_L = (S_{L_1}, S_{L_2}, \dots, S_{L_B})$ that reflects the theoretical label distribution. For each position j in the batch ($1 \leq j \leq B$), the pseudo-label is determined by

$$S_{L_j} = \min_{i \in \mathcal{B}} \left(y_i \cdot \theta \left(\sum_{k=1}^i n'_k - j \right) \right),$$

where $\mathcal{B} = \{1, 2, \dots, B\}$ denotes the set of batch indices. Here, $\theta(x)$ represents the unit step function. Essentially, this procedure replicates each label y_i according to its adjusted frequency n'_i . For instance, if the label set is (40, 50, 60) with adjusted frequencies (1, 2, 3), the resulting pseudo-label sequence is (40, 50, 50, 60, 60, 60). The pseudo-prediction sequence \mathcal{S}_P is obtained by sorting the model predictions in the batch. To ensure differentiability, we employ the fast differentiable sorting method described in Blondel et al. [2020].

The overall loss function is then defined as

$$L_{\text{Dist}} = \text{MAE}(\mathbf{Y}, \hat{\mathbf{Y}}) + \text{MAE}(\mathcal{S}_L, \mathcal{S}_P),$$

where \mathbf{Y} and $\hat{\mathbf{Y}}$ denote the ground truth labels and the model predictions, respectively. The first term ensures the accuracy of individual sample predictions, while the second term minimizes the discrepancy between the distribution of

predictions and the true label distribution. This formulation mitigates the tendency of traditional regression models to overly focus on the majority region, thereby reducing the bias that causes samples in low-sample regions to be predicted toward the dense central region.

In this context, the pseudo-labels and pseudo-predictions can be understood as effective representations of the corresponding distributions. 1. To illustrate this, imagine plotting histograms for both the pseudo-labels and pseudo-predictions, where the horizontal axis represents the labels and the vertical axis indicates their frequency. These histograms would reflect the underlying distribution of the labels and predictions. Therefore, the proposed method serves as an approximation of the true label and prediction distributions.

3.2.3 Experimental setup

The model was implemented using the PyTorch 2.2 framework and trained on an NVIDIA GeForce RTX 4090 GPU (24GB memory). The training process spanned 80 epochs, utilizing the Adam optimizer with an initial learning rate of $3e-3$. To enhance training stability, we employed a large batch size of 2,048 and applied L2 weight regularization with a factor of $\lambda = 1 \times 10^{-4}$ to mitigate overfitting. For the Dist loss calculation, Gaussian KDE was used with a bandwidth parameter of $\sigma = 0.5$ to model the age label distribution, which spans 21 to 111 years. Model performance was tracked using the MAE as the primary evaluation metric throughout the training.

3.2.4 Model interpretability

To enhance the interpretability of the model, this study employs saliency maps to visualize the regions of the PPG signals that the model prioritizes when predicting vascular age. Saliency maps are generated by computing the gradients of the input signal with respect to the model’s output, thereby highlighting the model’s sensitivity to various components of the signal during prediction. Specifically, regions exhibiting larger gradient magnitudes are indicative of areas that exert a stronger influence on the model’s prediction. To refine the visual clarity, Gaussian smoothing and interpolation techniques are applied to the saliency maps, minimizing noise and improving the discernibility of relevant signal features.

3.3 Outcome definition

This study incorporates several outcome definitions from the UKB dataset, including the primary outcome MACCE and secondary outcomes such as mortality, HF, MI, stroke, CHD, hypertension, and diabetes. MACCE is a composite endpoint comprising mortality, HF, MI, and stroke. Mortality data were obtained from the National Death Registries of the United Kingdom, while MI and stroke outcomes were derived from algorithmically defined criteria. Diagnoses for HF, CHD, hypertension, and diabetes were based on first occurrences. Specifically, CHD outcomes include angina pectoris, acute MI, subsequent MI, complications following acute MI, other acute ischemic heart diseases, and chronic ischemic heart disease. Hypertension encompasses both essential and secondary forms. Diabetes is categorized into insulin-dependent, non-insulin-dependent, malnutrition-related, other specified types, and unspecified diabetes mellitus.

3.4 Serial PPG analysis

Given that some participants in the UKB dataset attended multi-time point assessments, resulting in serial PPG data across different time points, we further investigated the application of AI-vascular age in such serial PPG data. Following the exclusion criteria outlined in Figure 2, all serial PPG data were excluded from the model development set, leaving 58,232 PPG records from 27,108 participants. Our analysis specifically focused on two distinct time points of serial PPG data: for participants with more than two PPG records, we selected their first two PPG data for analysis. In this analysis, we divided the participants into four groups based on the vascular age gap at the two time points: G1 (overestimation at both time points), G2 (underestimation or correct prediction at the first time point and overestimation at the second), G3 (overestimation at the first time point and underestimation or correct prediction at the second), and G4 (underestimation or correct prediction at both time points). We studied the differences in the risk of future incident MACCE across these groups.

3.5 Statistical analysis

To assess the consistency between AI-vascular age and calendar age, we calculated Pearson correlation coefficients and the MAE. We introduced the vascular age gap, defined as the difference between AI-vascular age and calendar age. This metric was then used to evaluate the clinical utility of AI-vascular age. To explore its predictive value, we performed multivariable-adjusted Cox proportional hazards regression analyses. In the UKB cohort, confounding variables were adjusted in two hierarchical models: Model 1 included age, sex, ethnicity, and BMI; Model 2 further adjusted for

hypertension, diabetes, dyslipidemia, smoking status, and CKD. For the MIMIC mortality set, adjustments were limited to age, sex, and ethnicity due to data limitations, with BMI excluded due to missing height information in a significant proportion of the patient population.

In the UKB survival analysis, participants with missing BMI data or those lost to follow-up were excluded from the clinical evaluation cohort, resulting in a study population of 111,561 participants and 141,745 PPG records. For censored cases without observed events, follow-up was administratively censored as of December 31, 2022. The log-rank test was employed to compare KM curves.

4 Discussion

In this study, we developed a CNN to predict vascular age directly from PPG signals. The model was trained and evaluated on the UKB dataset and externally validated using the MIMIC subset from the PulseDB dataset. To assess deviations in vascular aging, we introduced the vascular age gap, defined as the difference between AI-predicted vascular age and calendar age, based on a single PPG measurement. Our findings demonstrate that the vascular age gap serves as an independent risk factor for the primary outcome, MACCE, and secondary outcomes such as mortality, HF, MI, stroke, CHD, hypertension, and diabetes within the UKB cohort. External validation using the MIMIC subset further revealed that the vascular age gap is significantly associated with the risk of in-hospital mortality, suggesting its potential clinical application in both the general population and critically ill patients.

We also conducted an analysis of serial PPG measurements within the UKB cohort. Participants were categorized into four groups based on vascular age gap classifications at two time points: G1 (overestimation in both measurements), G2 (not overestimation in the first measurement but overestimation in the second), G3 (overestimation in the first measurement but not in the second), and G4 (not overestimation in either measurement). Compared to G4, participants in the other groups exhibited significantly higher risks for future MACCE events: G1 (HR 5.53, 95% CI: 2.73–11.23, $p < 0.005$), G2 (HR 3.63, 95% CI: 1.86–7.06, $p < 0.005$), and G3 (HR 3.02, 95% CI: 2.21–4.13, $p < 0.005$). The HR showed a progressively increasing trend from G3 to G1. This pattern may reflect the cumulative effect of vascular aging. G1 participants consistently displayed advanced vascular aging across both measurements, signifying prolonged exposure to poor cardiovascular health and the highest overall risk. In G2, the transition to overestimation during the second measurement suggests an accelerated progression of vascular aging, which reflects a recent deterioration in cardiovascular health. Consequently, their risk is elevated but remains lower than that of G1. For G3, although the second measurement indicates improvement in cardiovascular health, the long-term effects of previous excessive vascular aging may persist, leading to a moderately increased risk compared to G4, but still lower than G2.

To address the common challenge of data imbalance in regression tasks, particularly the age imbalance in the UKB dataset, we propose a novel loss function, Dist Loss. This method aligns the distribution of model predictions with the ground truth label distribution, effectively mitigating the risk of over-predicting samples from underrepresented regions into areas with higher label density. Our approach provides a straightforward and effective solution for handling imbalanced data distributions, offering a practical and reliable method for regression tasks under such conditions.

In tackling the interpretability challenges often associated with deep learning models, this study utilizes saliency map visualizations to identify areas of focus within the input signals. The results reveal that the model predominantly concentrates on the region around the diastolic peak of the PPG waveform when predicting vascular age, with secondary emphasis on the systolic peak. These findings are consistent with observed variations in the average PPG waveforms across different age groups. This approach provides a useful framework for understanding and explaining the model's prediction behavior, supporting conclusions from existing research.

CVDs are a leading global health threat, and individuals' ability to understand and manage their cardiovascular health is crucial in reducing the societal burden of these diseases. The aging population has contributed to a steady rise in the incidence of cardiovascular conditions, underscoring the increasing need for early screening and diagnosis. The widespread adoption of wearable devices has made PPG signals, due to their non-invasive, convenient, and continuous monitoring capabilities, an increasingly important tool in cardiovascular health management. Research focusing on cardiovascular diseases using PPG signals has gained traction in recent years. Studies have explored the relationship between PPG signals and vascular aging, with some indicating that increased arterial stiffness due to vascular aging can lead to the disappearance of the dicrotic notch and inflection points in PPG waveforms. Most previous research has relied on traditional feature engineering methods to extract parameters such as the reflection index from PPG signals to study their relationship with cardiovascular diseases. However, these manually extracted parameters are not always intuitive, and the reliance on specialized knowledge limits their broader application in personalized cardiovascular health management. Thus, there is a growing need for more intuitive and easily interpretable cardiovascular health indicators for individuals.

Unlike traditional waveform parameters such as pulse wave velocity, age is a highly intuitive and easily understood metric, widely applicable in clinical settings. By leveraging PPG signals, an indicator reflecting vascular aging offers substantial value in practical applications. Building upon this concept, this study proposes using deep learning techniques to predict vascular age directly from PPG signals, thus quantifying the degree of vascular aging. This approach provides a straightforward, actionable, and easily understandable cardiovascular health indicator. The underlying rationale is that increased arterial stiffness due to vascular aging induces changes in the PPG waveform, embedding information on vascular aging within the signal. Through validation across multiple datasets, we demonstrate the utility of this vascular age indicator in both single and serial PPG measurements. Furthermore, its association with in-hospital mortality highlights its potential value in critically ill patients. This vascular age indicator is easily accessible, as it can be obtained through devices such as smart wristbands. Its intuitive nature further enhances its practical application. In daily life, individuals can use this indicator to gain a better understanding of their cardiovascular health, potentially prompting proactive cardiovascular disease screenings. In clinical settings, this indicator can assist healthcare professionals in evaluating a patient’s hemodynamic status, guiding intervention strategies to improve patient outcomes.

5 Conclusion

This study introduces an accessible and intuitive physiological age indicator that reflects an individual’s cardiovascular health status. Preliminary results support its potential application in both the general population and critically ill patients. Future research will focus on further exploring the clinical value of the AI-based vascular age indicator from several perspectives: 1) Investigating its relationship with specific cardiovascular diseases; 2) Exploring its application in long-term continuous monitoring, leveraging the richer data obtained from such monitoring; and 3) Conducting deeper validation of the indicator’s significance in real-world settings, offering actionable health management solutions and potential interventions.

Data Availability

This study used data from the UKB, which is globally accessible to approved researchers (<http://ukbiobank.ac.uk/register-apply/>). UKB has obtained ethical approval from the North West-Haydock Research Ethics Committee (REC reference: 21/NW/0157). This study was approved by the UKB under application 90018. The PulseDB dataset is publicly available at <https://github.com/pulselabteam/PulseDB>. Access to the MIMIC-III Clinical Database requires completion of the Collaborative Institutional Training Initiative course and approval from PhysioNet (<https://physionet.org/content/mimiciii/1.4>).

The implementation of Dist Loss is available in the GitHub repository at <https://github.com/Ngk03/Dist-Loss>. The model configuration and pretrained weights can be found at <https://huggingface.co/Ngks03/PPG-VascularAge>.

Acknowledgement

This work was supported by the Beijing Natural Science Foundations (QY23040); National Natural Science Foundation of China (62102008).

References

- Gregory A Roth, Degu Abate, Kalkidan Hassen Abate, Solomon M Abay, Cristiana Abbafati, Nooshin Abbasi, Hedayat Abbastabar, Foad Abd-Allah, Jemal Abdela, Ahmed Abdelalim, et al. Global, regional, and national age-sex-specific mortality for 282 causes of death in 195 countries and territories, 1980–2017: a systematic analysis for the global burden of disease study 2017. *The lancet*, 392(10159):1736–1788, 2018.
- Cyrus Cooper. Global, regional, and national disability-adjusted life-years (daly) for 359 diseases and injuries and health life expectancy (hale) for 195 countries and territories, 1990-2017: A systematic analysis for the global burden of disease study 2017. *The Lancet*, 392(10159):1859–1922, 2018.
- George A Mensah, Gregory A Roth, and Valentin Fuster. The global burden of cardiovascular diseases and risk factors: 2020 and beyond, 2019.
- Megan Lindstrom, Nicole DeCleene, Henry Dorsey, Valentin Fuster, Catherine O Johnson, Kate E LeGrand, George A Mensah, Christian Razo, Benjamin Stark, Justine Varieur Turco, et al. Global burden of cardiovascular diseases and risks collaboration, 1990-2021. *Journal of the American College of Cardiology*, 80(25):2372–2425, 2022.

- Kim Robin van Daalen, Dudan Zhang, Stephen Kaptoge, Ellie Paige, Emanuele Di Angelantonio, and Lisa Pennells. Risk estimation for the primary prevention of cardiovascular disease: considerations for appropriate risk prediction model selection. *The Lancet Global Health*, 12(8):e1343–e1358, 2024.
- Birgit Vogel, Monica Acevedo, Yolande Appelman, C Noel Bairey Merz, Alaide Chieffo, Gemma A Figtree, Mayra Guerrero, Vijay Kunadian, Carolyn SP Lam, Angela HEM Maas, et al. The lancet women and cardiovascular disease commission: reducing the global burden by 2030. *The Lancet*, 397(10292):2385–2438, 2021.
- Vivek Pandey, Umesh Kumar Lilhore, and Ranjan Walia. A systematic review on cardiovascular disease detection and classification. *Biomedical Signal Processing and Control*, 102:107329, 2025.
- TA Addissouky, I El Tantawy El Sayed, MM Ali, MH Alubiady, and Y Wang. Recent developments in the diagnosis, treatment, and management of cardiovascular diseases through artificial intelligence and other innovative approaches. *J Biomed Res*, 5(1):29–40, 2024.
- Pankaj, Ashish Kumar, Rama Komaragiri, and Manjeet Kumar. A review on computation methods used in photoplethysmography signal analysis for heart rate estimation. *Archives of Computational Methods in Engineering*, 29(2): 921–940, 2022.
- Christina Schröder, Robert Förster, Daniel R Zwahlen, and Paul Windisch. The apple watch spo2 sensor and outliers in healthy users. *NPJ Digital Medicine*, 6(1):63, 2023.
- Tania Pereira, Nate Tran, Kais Gadhomi, Michele M Pelter, Duc H Do, Randall J Lee, Rene Colorado, Karl Meisel, and Xiao Hu. Photoplethysmography based atrial fibrillation detection: a review. *NPJ digital medicine*, 3(1):1–12, 2020.
- Gareth J Williams, Abdulaziz Al-Baraikhan, Frank E Rademakers, Fabio Ciravegna, Frans N van de Vosse, Allan Lawrie, Alexander Rothman, Euan A Ashley, Martin R Wilkins, Patricia V Lawford, et al. Wearable technology and the cardiovascular system: the future of patient assessment. *The Lancet Digital Health*, 5(7):e467–e476, 2023.
- Chayakrit Krittanawong, Albert J Rogers, Kipp W Johnson, Zhen Wang, Mintu P Turakhia, Jonathan L Halperin, and Sanjiv M Narayan. Integration of novel monitoring devices with machine learning technology for scalable cardiovascular management. *Nature Reviews Cardiology*, 18(2):75–91, 2021.
- Chengming Yang, Cesar Veiga, Juan J Rodriguez-Andina, Jose Farina, Andres Iniguez, and Shen Yin. Using ppg signals and wearable devices for atrial fibrillation screening. *IEEE Transactions on Industrial Electronics*, 66(11): 8832–8842, 2019.
- Mohamed Elgendi, Richard Fletcher, Yongbo Liang, Newton Howard, Nigel H Lovell, Derek Abbott, Kenneth Lim, and Rabab Ward. The use of photoplethysmography for assessing hypertension. *NPJ digital medicine*, 2(1):60, 2019.
- Seyedeh Somayyeh Mousavi, Mohammad Firouzmand, Mostafa Charmi, Mohammad Hemmati, Maryam Moghadam, and Yadollah Ghorbani. Blood pressure estimation from appropriate and inappropriate ppg signals using a whole-based method. *Biomedical Signal Processing and Control*, 47:196–206, 2019.
- Ramachandran S Vasani, Meghan I Short, Teemu J Niiranen, Vanessa Xanthakis, Charles DeCarli, Susan Cheng, Sudha Seshadri, and Gary F Mitchell. Interrelations between arterial stiffness, target organ damage, and cardiovascular disease outcomes. *Journal of the American Heart Association*, 8(14):e012141, 2019.
- Ramachandran S Vasani, Stephanie Pan, Vanessa Xanthakis, Alexa Beiser, Martin G Larson, Sudha Seshadri, and Gary F Mitchell. Arterial stiffness and long-term risk of health outcomes: the framingham heart study. *Hypertension*, 79(5): 1045–1056, 2022.
- Yunlong Li, Yang Xu, Zuchang Ma, Yuqi Ye, Lisheng Gao, and Yining Sun. An xgboost-based model for assessment of aortic stiffness from wrist photoplethysmogram. *Computer methods and programs in biomedicine*, 226:107128, 2022.
- Yawei Chen, Xuezhi Yang, Rencheng Song, Xuenan Liu, and Jie Zhang. Predicting arterial stiffness from single-channel photoplethysmography signal: a feature interaction-based approach. *IEEE Journal of Biomedical and Health Informatics*, 2024.
- Emilly M Lima, Antônio H Ribeiro, Gabriela MM Paixão, Manoel Horta Ribeiro, Marcelo M Pinto-Filho, Paulo R Gomes, Derick M Oliveira, Ester C Sabino, Bruce B Duncan, Luana Giatti, et al. Deep neural network-estimated electrocardiographic age as a mortality predictor. *Nature communications*, 12(1):5117, 2021.
- Hanjin Park, Oh-Seok Kwon, Jaemin Shim, Daehoon Kim, Je-Wook Park, Yun-Gi Kim, Hee Tae Yu, Tae-Hoon Kim, Jae-Sun Uhm, Jong-Il Choi, et al. Artificial intelligence estimated electrocardiographic age as a recurrence predictor after atrial fibrillation catheter ablation. *NPJ Digital Medicine*, 7(1):234, 2024.
- Philip Hempel, Antônio H Ribeiro, Marcus Vollmer, Theresa Bender, Marcus Dörr, Dagmar Krefting, and Nicolai Spicher. Explainable ai associates ecg aging effects with increased cardiovascular risk in a longitudinal population study. *npj Digital Medicine*, 8(1):25, 2025.

- Q Yousef, MBI Reaz, and Mohd Alauddin Mohd Ali. The analysis of ppg morphology: investigating the effects of aging on arterial compliance. *Measurement Science Review*, 12(6):266–271, 2012.
- Wan-Hua Lin, Dingchang Zheng, Guanglin Li, and Fei Chen. Age-related changes in blood volume pulse wave at fingers and ears. *IEEE Journal of Biomedical and Health Informatics*, 2023.
- Cathie Sudlow, John Gallacher, Naomi Allen, Valerie Beral, Paul Burton, John Danesh, Paul Downey, Paul Elliott, Jane Green, Martin Landray, et al. Uk biobank: an open access resource for identifying the causes of a wide range of complex diseases of middle and old age. *PLoS medicine*, 12(3):e1001779, 2015.
- Weinan Wang, Pedram Mohseni, Kevin L Kilgore, and Laleh Najafizadeh. Pulsedb: A large, cleaned dataset based on mimic-iii and vitaldb for benchmarking cuff-less blood pressure estimation methods. *Frontiers in Digital Health*, 4: 1090854, 2023.
- Alistair EW Johnson, Tom J Pollard, Lu Shen, Li-wei H Lehman, Mengling Feng, Mohammad Ghassemi, Benjamin Moody, Peter Szolovits, Leo Anthony Celi, and Roger G Mark. Mimic-iii, a freely accessible critical care database. *Scientific data*, 3(1):1–9, 2016a.
- Hyung-Chul Lee, Yoonsang Park, Soo Bin Yoon, Seong Mi Yang, Dongnyeok Park, and Chul-Woo Jung. Vitaldb, a high-fidelity multi-parameter vital signs database in surgical patients. *Scientific Data*, 9(1):279, 2022.
- Alistair Johnson, Tom Pollard, and Roger Mark. Mimic-iii clinical database (version 1.4). *PhysioNet*, 10(C2XW26):2, 2016b.
- Shenda Hong, Yanbo Xu, Alind Khare, Satria Priambada, Kevin Maher, Alaa Aljiffry, Jimeng Sun, and Alexey Tumanov. Holmes: Health online model ensemble serving for deep learning models in intensive care units. In *Proceedings of the 26th ACM SIGKDD International Conference on Knowledge Discovery & Data Mining*, pages 1614–1624, 2020.
- Kaiming He, Xiangyu Zhang, Shaoqing Ren, and Jian Sun. Deep residual learning for image recognition. In *Proceedings of the IEEE conference on computer vision and pattern recognition*, pages 770–778, 2016.
- Jie Hu, Li Shen, and Gang Sun. Squeeze-and-excitation networks. In *Proceedings of the IEEE conference on computer vision and pattern recognition*, pages 7132–7141, 2018.
- Emanuel Parzen. On estimation of a probability density function and mode. *The annals of mathematical statistics*, 33(3):1065–1076, 1962.
- Mathieu Blondel, Olivier Teboul, Quentin Berthet, and Josip Djolonga. Fast differentiable sorting and ranking. In *International Conference on Machine Learning*, pages 950–959. PMLR, 2020.